CHEMISTRY
A EUROPEAN JOURNAL

DOI: 10.1002/chem.200701412

Octahedral Adducts of Dichlorosilane with Substituted Pyridines: Synthesis, Reactivity and a Comparison of Their Structures and ^{29}Si NMR Chemical Shifts

Gerrit W. Fester,[a] Jörg Wagler,[a] Erica Brendler,[b] Uwe Böhme,[a] Gerhard Roewer,[a] and Edwin Kroke*[a]

Abstract: H_2SiCl_2 and substituted pyridines (Rpy) form adducts of the type all-*trans*-SiH_2Cl_2·2 Rpy. Pyridines with substituents in the 4- (CH_3, C_2H_5, H_2C=CH, $(CH_3)_3C$, $(CH_3)_2N$) and 3-positions (Br) give the colourless solids **1a–f**. The reaction with pyrazine results in the first 1:2 adduct (**2**) of H_2SiCl_2 with an electron-deficient heteroaromatic compound. Treatment of **1d** and **1e** with $CHCl_3$ yields the ionic complexes $[SiH_2(Rpy)_4]Cl_2$·6 $CHCl_3$ (Rpy = 4-methylpyridine (**3d**) and 4-ethylpyridine (**3e**)). All products are investigated by single-crystal X-ray diffraction and ^{29}Si CP/MAS NMR spectroscopy. The Si atoms are found to be situated on centres of symmetry (inversion, rotation), and the Si–N distances vary between 193.3 pm for **1c** (4-(dimethylamino)pyridine complex) and 197.3 pm for **2**. Interestingly, the pyridine moieties are coplanar and nearly in an eclipsed position with respect to the SiH_2 units, except for the ethyl-substituted derivative **1e**, which shows a more staggered conformation in the solid state. Calculation of the energy profile for the rotation of one pyridine ring indicates two minima that are separated by only 1.2 kJ mol^{-1} and a maximum barrier of 12.5 kJ mol^{-1}. The ^{29}Si NMR chemical shifts (δ_{iso}) range from −145.2 to −152.2 ppm and correlate with the electron density at the Si atoms, in other words with the +I and +M effects of the substituents. Again, compound **1e** is an exception and shows the highest shielding. The bonding situation at the Si atoms and the ^{29}Si NMR tensor components are analysed by quantum chemical methods at the density functional theory level. The natural bond orbital analysis indicates polar covalent Si–H bonds and very polar Si–Cl bonds, with the highest bond polarisation being observed for the Si–N interaction, which must be considered a donor–acceptor interaction. An analysis of the topological properties of the electron distribution (AIM) suggests a Lewis structure, thereby supporting this bonding situation.

Keywords: hypercoordination · NMR spectroscopy · quantum chemistry · silicon · X-ray diffraction

Introduction

The tendency of the chlorosilanes SiH_nCl_{4-n} to form coordination compounds with tertiary amines appears to be a good way of studying their Lewis acidity, although only a few compounds of this type have been synthesised to date.[1–4] Most of these chlorosilane–amine adducts are only stable in the solid state and dissociate quantitatively on melting, dissolution, or evaporation,[5] which explains why only limited information about their molecular structure is available. The adducts described in the literature mainly involve those with unsubstituted or methyl-substituted pyridines as donor molecules.[6]

The relative stability of such octahedral complexes depends on the basicity of the Lewis base, the energy difference between the tetrahedral and the planar structures of H_2SiCl_2[7] as well as the steric demands of the donor molecules and the resulting intramolecular repulsive interactions.

Dismutation reactions of chlorosilanes in the presence of amine bases are also known. For example, an Si–H dismutation process occurs when SiH_3Cl is added to an excess of

[a] G. W. Fester, Dr. J. Wagler, Dr. U. Böhme, Prof. Dr. G. Roewer, Prof. Dr. E. Kroke
Institut für Anorganische Chemie, TU Bergakademie Freiberg
Leipziger Strasse 29, 09596 Freiberg (Germany)
Fax: (+49) 3731-39-4058
E-mail: kroke@chemie.tu-freiberg.de

[b] Dr. E. Brendler
Institut für Analytische Chemie, TU Bergakademie Freiberg
Leipziger Strasse 29, 09596 Freiberg (Germany)

pyridine to give a hexacoordinate silicon complex[3] [Eq. (1)]:

$$2\,SiH_3Cl + 2\,NC_5H_5 \rightarrow SiH_2Cl_2(NC_5H_5)_2 + SiH_4 \quad (1)$$

Another route to hexacoordinate SiH_2Cl_2 derivatives is based on the decomposition of $NMe(SiHCl_2)_2$ into the dichlorosilane pyridine complex and a mixture of by-products by the action of tertiary amines[5] [Eq. (2)]:

$$NMe(SiHCl_2)_2 + 2\,NC_5H_5 \rightarrow SiH_2Cl_2(NC_5H_5)_2 + 1/n(\text{-}SiCl_2\text{-}NMe\text{-})_n \quad (2)$$

These reactions suggest that H_2SiCl_2 is a suitable Lewis acid for complex formation with pyridines, tertiary amines and other Lewis bases, and this result was recently supported theoretically and compared to the Lewis acidity of related compounds such as $SiCl_4$, SiH_4 and GeF_4.[8] This suggestion is further supported by an unexpected redistribution reaction of trichlorosilane. This redistribution occurs in the presence of *N*,*N*,*N*′,*N*′-tetraethylethylenediamine (teeda) and leads to an octahedral dichlorosilane complex with $SiH_2Cl_2N_2$ coordination,[9] as shown in Equation (3):

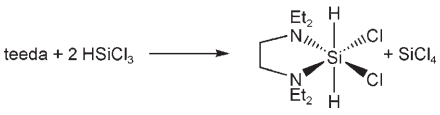

(3)

Herein we report the systematic synthesis and investigation of the hexacoordinate compounds $H_2SiCl_2(Rpy)_2$, which exhibit various substitution patterns at the donor molecule. These solid adducts are stable at room temperature and are directly accessible from dichlorosilane.

Results and Discussion

Synthesis and structural characterisation of 1a–f and 2: Compounds **1a–f** and **2** (Scheme 1) were synthesised in aprotic solvents such as *n*-hexane, toluene or THF. There was no indication for the formation of dichlorosilane/solvent complexes. 2,6-Disubstituted pyridines, such as 2,6-dimethylpyridine (lutidine) and 2,4,6-trimethylpyridine (collidine), do not form octahedral silicon complexes, nor does 2-vinylpyridine. We initially expected the formation of octahedrally coordinated silicon compounds in analogy to the complexation of H_2SiCl_2 with 2,4-dimethylpyridine.[6] The steric demands of the 2,6-dimethyl and 2-vinyl substituents may be responsible for this lack of reactivity.

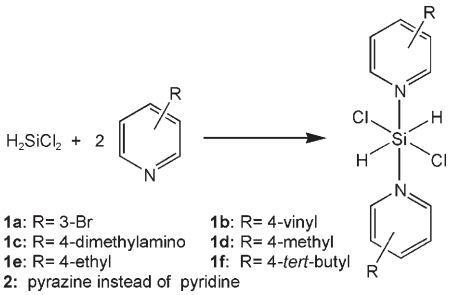

Scheme 1. The reaction of dichlorosilane with substituted pyridines.

The hexacoordinate silicon complexes were characterised by CP/MAS NMR spectroscopy, single-crystal X-ray diffraction and Raman spectroscopy. The low solubilities of the compounds reported herein precluded their characterisation by solution NMR spectroscopy. As expected, all seven compounds **1a–f** and **2** exhibit a characteristic Si–H valence vibration band at 2050–2103 cm^{-1} in the Raman spectrum (see Table 1). The ^{29}Si NMR chemical shifts are all around $\delta =$ −145 ppm, which is characteristic for octahedral silicon compounds.[10] The Si atoms gain electron density with increasing +M and/or +I effects of the substituents at the pyridine moiety, which leads to a high-field shift of the ^{29}Si NMR signal. This is most obvious for **1c** due to the strong +M effect of the dimethylamino substituent (Scheme 2).

Table 1. ^{29}Si CP/MAS NMR spectroscopic data, selected bond lengths and ν(SiH) resonance bands for compounds **1a–f**, **2** and H_2SiCl_2 (compounds are ordered according to their ^{29}Si NMR shift).

	R	δ_{iso} ^{29}Si [ppm]	*d*(Si–N) [pm]	*d*(Si–Cl) [pm]	ν(SiH) [cm^{-1}]
H_2SiCl_2		−11.3		204.8(8)	2200[8]
	H	−145.1	196.9(1)[5]	228.8(1)	2075
1a	3-Br	−145.2	196.9(1)	228.1(1)	2103
1b	4-$CHCH_2$	−147.2	195.6(1)	228.5(1)	2078
1d	4-CH_3	−148.8	196.6(1)	227.5(1)	2080
2		−148.9	197.3(1)	226.7(1)	2094
1f	4-$C(CH_3)_3$	−149.5	196.3(1)	226.9(1)	2075
1c	4-$[N(CH_3)_2]$	−151.8	193.1(3)	230.3(1)	2050
1e	4-CH_2CH_3	−152.2	195.9(1)	227.7(1)	2061

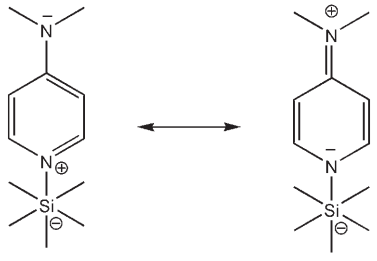

Scheme 2. Mesomeric effects of substituents in 4-(dimethylamino)pyridine adduct **1c**.

A decrease of the ν(Si-H) wavenumber correlates with a decrease of the Si–N bond length (Table 1). This is due to an increase of the electron-donating capacity of the pyridine base, which is highest for the $[N(CH_3)_2]$ substituent, lowest

for the Br substituent and intermediate for the alkyl-substituted pyridines.

As shown by the X-ray structural data (see below), the pyridine moiety of compound **1c** exhibits a quinoid resonance structure unlike the remaining octahedral complexes, which have bond lengths typical of aromatic pyridine rings. The 4-ethyl-substituted derivative **1e** is the only compound which obviously does not match the M/I effect induced trend of the ^{29}Si NMR chemical shifts. This is most likely caused by the special molecular conformation of **1e** (see below), that is, the torsion angle between the pyridine rings. A more detailed analysis of the ^{29}Si NMR spectroscopic data is provided later in this discussion (measurement and calculation of the ^{29}Si NMR chemical shift tensor).

All $(Rpy)_2SiH_2Cl_2$ complexes **1a–f** crystallise in centrosymmetric space groups and with half of a molecule as the asymmetric unit in each case. The molecular structures of **1a**, **1b**, **1d** and **1f** are depicted in Figure 1. The pyridine N-

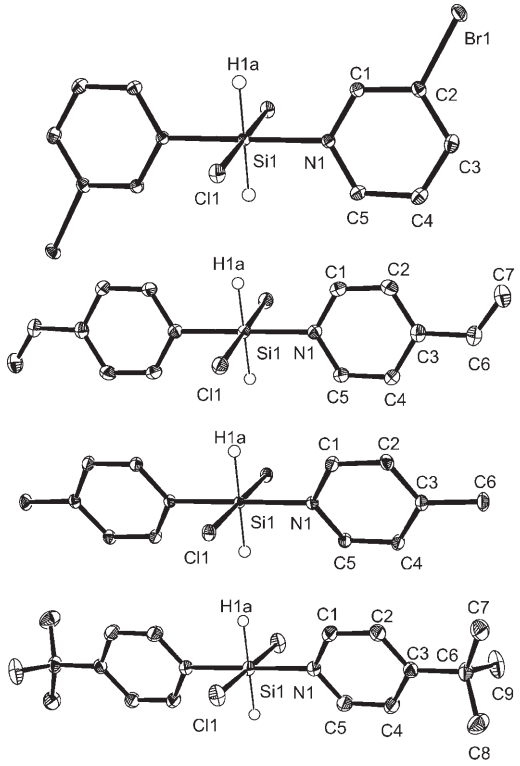

Figure 1. Molecular structures of (top to bottom) **1a**, **1b**, **1d** and **1f** (ORTEP plots with 50% probability ellipsoids; C-bonded hydrogen atoms omitted for clarity). Selected bond lengths are provided in Tables 1 and 2.

atoms, silane H-atoms and Cl atoms in these adducts are situated *trans* to each other in a pattern that makes these complexes structurally related to the adducts (pyridine)$_2SiH_2Cl_2$,[5] (3-methylpyridine)$_2SiH_2Cl_2$[5] and (2,4-dimethylpyridine)$_2SiH_2Cl_2$.[6]

Complex **1c** crystallises as the chloroform solvate **1c**·2 $CHCl_3$ (Figure 2) and the chloroform molecules may

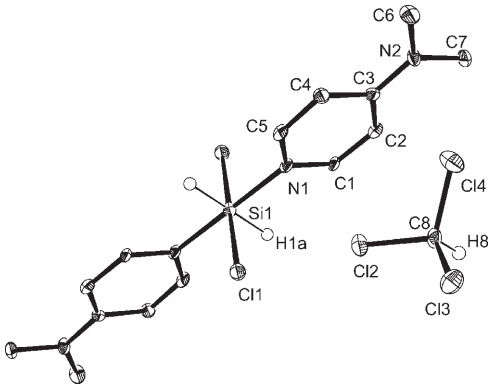

Figure 2. Molecular structure of **1c**·2 $CHCl_3$ (ORTEP plot with 50% probability ellipsoids; most hydrogen atoms omitted for clarity). Selected bond lengths are summarised in Tables 1 and 2.

play a role in achieving a dense molecular packing due to the modified steric demands of the substituent at the pyridine system. Intermolecular interactions, however, are also found: the C8–H8 bond points towards chlorine atom Cl1 of a neighbouring molecule ($Cl_3C–H\rightarrow Cl$ distance of 2.61 Å; Table 2).

The common features of the three previously published complexes[5,6] and the pyridine adducts **1a–f** are the coplanar arrangement of the two pyridine ring systems, the slight out-of-plane position of the Si–H bonds and the orthogonal arrangement of the chlorine atoms with respect to the SiH_2 unit (Figure 3, left). This preferred conformation can be interpreted as a result of only small repulsive interactions between the Si-bonded H atoms and the pyridine H atoms in the 2-position. Thus, substitution of Si–H for Si–X moieties leads to significant out-of-plane positions of all four substituents, as can easily be seen in the structures of the pyridine adducts of $SiCl_4$.[11,12]

Contrasting the conformational behaviour of the compounds discussed above, the Si atom of complex **1e** is not situated on a centre of inversion and its H-Si-H axis is located on a twofold axis of rotation, which means that the pyridine ring systems are not coplanar (Figure 3, right, Figure 4). Despite this conformational difference, the coordination behaviour of the pyridine ligand (Si–N separation) is similar to those in complexes **1a**, **1b**, **1d** and **1f**.

All complexes have five independent pyridine carbon atoms in the solid state, although C2,6 and C3,5 are not always resolved in the ^{13}C CP/MAS NMR spectrum (see Experimental Section).

Compound **1b** was chosen as a representative example to analyze the relative stabilities of the different conformations of the pyridine rings by quantum chemical methods. The torsion angle C5-N1-Si1-Cl1 was varied in 5° steps from 0 to 190° and the geometry of the molecule was optimised at every step with only the torsion angle fixed. The results of this potential energy surface (PES) scan are summarised in Figure 5. The local minimum at a torsion angle of 60° corresponds to the conformation found in the X-ray structure of **1b**. The solid-state structure, however, has a more "perpen-

Table 2. Selected bond lengths [pm] for **1a–f** and **2** (standard deviation in parentheses). The Si–N and Si–Cl bond lengths are summarised in Table 1.

	1a	1b	1c	1d	1e	1f	2
Si1–H1A	137(1)	140(2)	144(3)	137(1)	137(1)	139(2)	138(1)
Si1–H1B					141(1)		
N1–C1	134.3(1)	134.1(2)	134.4(4)	134.1(2)	134.1(1)	133.7(2)	133.1(1)
N1–C5	134.5(1)	134.4(2)	134.7(4)	134.7(1)	134.2(1)	133.7(2)	
C1–C2	138.0(1)	137.5(2)	135.4(5)	138.0(2)	138.5(1)	137.9(2)	138.3(1)
C2–C3	139.1(1)	139.8(2)	140.2(5)	139.6(2)	139.5(1)	138.9(2)	
C3–C4	138.4(1)	139.4(2)	141.6(5)	139.8(2)	139.6(1)	139.7(2)	138.2(1)
C4–C5	138.5(1)	137.5(2)	135.9(5)	138.3(2)	138.0(1)	137.5(2)	
C3–C6		132.2(2)		149.7(2)	150.1(1)	152.2(2)	
C6–C7					152.3(1)	153.2(2)	
C6–C8						153.1(2)	
C6–C9						153.3(2)	
N2–C3			134.4(4)				133.2(1)
N2–C2							133.5(1)
N2–C6			145.5(5)				
N2–C7			145.8(4)				

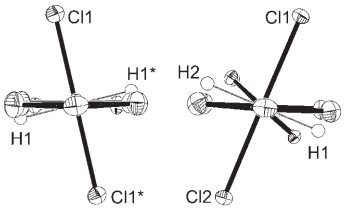

Figure 3. View along the N-Si-N axis in molecules **1b** (left) and **1e** (right). Ethyl- and vinyl groups as well as C-bonded hydrogen atoms have been omitted for clarity. The Cl1-Si1-N1-C5) dihedral angles are 76.4 (1)° (**1b**) and 70.2 (1)° (**1e**). The pyridine planes in **1e** are twisted with respect to each other by 39.67(2)°. The dihedral angles between the pyridine planes are 0° for the other molecules.

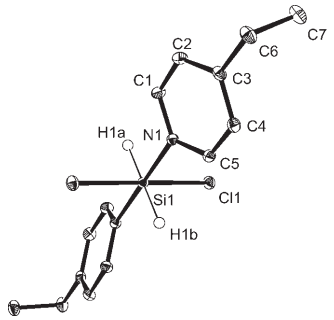

Figure 4. Molecular structure of **1e** (ORTEP plot with 50% probability ellipsoids; C-bonded hydrogen atoms omitted for clarity). Selected bond lengths are provided in Tables 1 and 2.

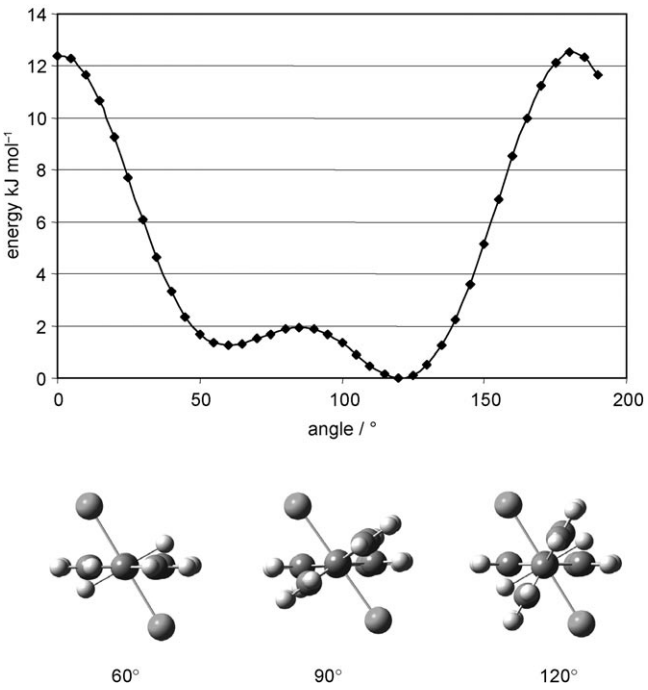

Figure 5. A representation of the PES scan of **1b** (top) and figures showing the rotation of one pyridine ring and a view along the N1–Si axis at different C5-N1-Si1-Cl1 torsion angles (bottom).

dicular" conformation, that is, the chlorine atoms are nearly perpendicular to the plane of the pyridine rings, with torsion angles of 76.4°. The difference between the calculated and experimentally determined torsion angles can be attributed to packing effects in the solid state.

There is a very flat energy barrier separating the local minimum at 60° from the global minimum at 120°. Such a "staggered" conformation is found for **1e** in the solid state. The energy difference between the rotamers at 60° and 120° is only 1.2 kJ mol^{-1}, which means that these two minima are nearly equivalent. Both conformations lead to minimal steric repulsion between the axial pyridine rings and the equatorial substituents at the silicon atom.

The overall energy barrier for rotation of the pyridine ring around the Si–N bond is about 12.5 kJ mol^{-1}, a value which is easily reached in solution at room temperature. A similar rather shallow energy potential has been found for $SiH_2Cl_2 \cdot 2\,Rpy$.[5] A global minimum at a torsion angle of 60.4° was calculated, which deviates only slightly from the value found in the solid state.

The Si–Cl bonds are also of similar length and the C–C/C–N bond systems of the pyridine ligands are comparable.

The influence of the dimethylamino group in complex **1c**, however, is striking. The formation of much shorter Si–N bonds causes significant lengthening of the Si–Cl bonds and the +M effect of the dimethylamino substituent leads to quinoid-type bond lengths in the pyridine system.

Complex **2**, which represents the first structurally characterised hexacoordinate silicon complex with a nitrogen-rich six-membered heterocycle as additional donor, also crystallises in a centrosymmetric space group ($P2_1/c$) with the Si atom situated on a centre of symmetry (Figure 6). The pyrazine ring systems are coplanar and even the Si–H and Si–Cl bonds are aligned in the same manner as in complexes **1a–f**. Due to the electron deficiency of the pyrazine ligand, the Si–N bond [197.3(1) pm] is significantly longer than in the pyridine adducts. This slightly stretched interatomic distance, however, is still notably shorter than the Si–N bond length in the adduct (2,4-dimethylpyridine)$_2$SiH$_2$Cl$_2$[6] (201.6 pm) as a result of the steric hindrance due to the methyl group in the 2-position.

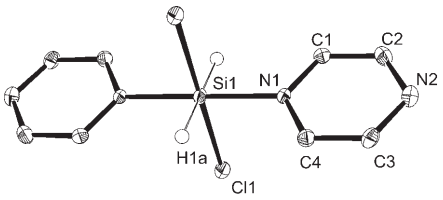

Figure 6. Molecular structure of **2** (ORTEP plot with 50% probability ellipsoids; C-bonded hydrogen atoms omitted for clarity).

Reactivity: As mentioned in the introduction, most hypercoordinate Lewis base adducts of chlorosilanes are only stable in the solid state and dissociate upon dissolution or heating (melting). A simple method to investigate the relative stabilities of SiH$_2$Cl$_2$·2 Rpy adducts involves exchange reactions using pyridines with different substituents. The observed exchange of the pyridine ligands upon treatment of the complex H$_2$SiCl$_2$·2 py with 4-(dimethylamino)pyridine suggests that **1c** is more stable:

$$H_2SiCl_2 \cdot 2\,py + 2(4\text{-DMAP}) \rightarrow H_2SiCl_2 \cdot 2\,(4\text{-DMAP}) + 2\,py \quad (4)$$

Exchange of the pyridine ligands was also observed in the absence of any other substituted pyridine ligands. Thus, the extraction of **1d** and **1e** with boiling $CHCl_3$ caused the formation of dicationic silicon complexes **3d** and **3e**, respectively, where both Si–Cl bonds have been substituted by the respective pyridine molecules (Scheme 3). The chloride counterions are stabilised by chloroform molecules. In contrast, the extraction of **1a–c** and **1f** with boiling $CHCl_3$ does not cause any ionisation of the Si–Cl bonds. Single crystals of **3d** and **3e** suitable for X-ray structure analyses were obtained (see Experimental Section). The extraction of **2** with boiling $CHCl_3$ or CH_3CN causes the complex to decompose.

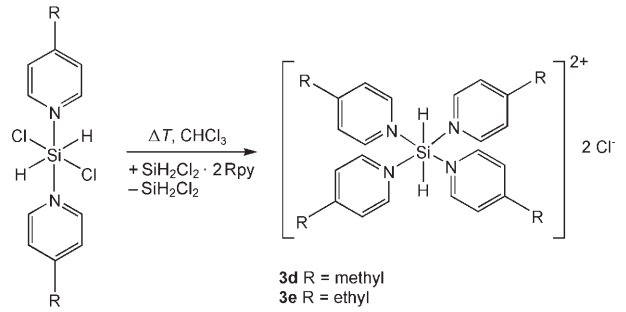

Scheme 3. Dissociation of **3d** and **3e** in boiling $CHCl_3$ to yield the adduct $[(Rpy)_4SiH_2]^{2+}$.

Kost et al. have shown that Si–X dissociation depends strongly on a variety of parameters, particularly temperature (ionisation is enhanced at low temperature), solvent (ionisation takes places in hydrogen-bond donor solvents) and the nature of the anion.[13,14] In the present case, the hydrogen-bond donor solvent $CHCl_3$ stabilises the chloride ion.

The crystal structure of **3d** has already been described by Bolte et al.[15] therefore it is not discussed further here. The crystal structure of **3e** (Figure 7) also contains half of the dication $[(4\text{-ethylpyridine})_4SiH_2]^{2+}$ as well as a chloride ion and three chloroform molecules in the asymmetric unit. In contrast to the structure of **1c**, the chloroform molecules solvate the chloride anion in the crystal of **3e**. Two of these chloroforms are rotationally disordered around their C–H bonds, which are directed towards the chloride ion. The same two molecules as well, as their symmetry equivalents, surround one ethyl group of the cation (C13–C14), which is necessarily also disordered due to the varying steric demands of the disordered solvent molecules. It is worth mentioning that the other ethyl group (C6–C7) seems unaffected even though some slightly disordered $CHCl_3$ molecules are found in close proximity (see Table 3 for bond lengths and angles of **3d** and **3e**).

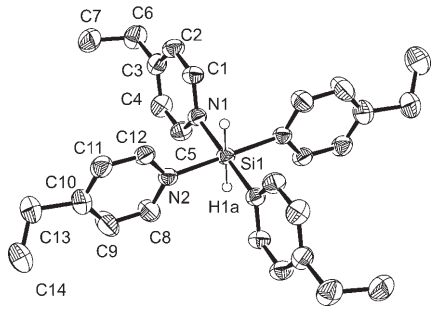

Figure 7. Structure of the dication $[(4\text{-Et-py})_4SiH_2]^{2+}$ in a crystal of **3e**·6 $CHCl_3$ (ORTEP plot with 50% probability ellipsoids; C-bonded hydrogen atoms omitted for clarity). Selected bond lengths and bond angles are provided in Table 3.

The overall configuration of the dication, the Si atom of which is located on a centre of symmetry, is related to the structures of the cations in the compounds [(4-methylpyridi-

Table 3. Selected bond lengths [pm] and angles [°] for **3d** and **3e** (standard deviations in parentheses).

	3d	3e
Si1–N1	196.0(1)	196.4(2)
Si1–N2	196.0(1)	196.3(2)
Si1–H1A	141(2)	138(2)
N1–C1	134.3(1)	134.0(3)
N1–C5	134.5(1)	134.8(3)
C1–C2	138.0(1)	137.5(2)
C2–C3	139.1(1)	139.8(2)
C3–C4	138.4(1)	139.4(2)
C4–C5	138.5(1)	137.5(2)
C3–C6	149.8(2)	150.7(3)
C6–C14	–	150.6(4)
N2–C7	134.8(1)	133.7(3)
N2–C11	134.5(1)	134.9(3)
C10–C11	138.0(2)	137.3(4)
C7–C8	137.7(2)	139.2(4)
C8–C9	139.5(2)	137.8(4)
C9–C10	139.1(2)	136.9(3)
C9–C12	149.5(2)	153.9(4)
C12–C13	–	146.6(7)
H1A-Si1-N1	89.2(7)	90.5(9)
H1A-Si1-N2	89.4(7)	90.6(9)

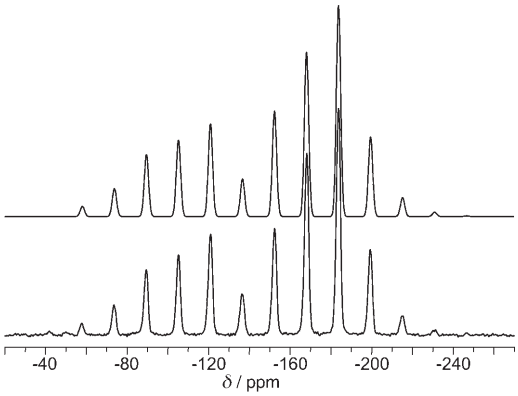

Figure 8. Top: ^{29}Si CP/MAS spectrum of **1e** calculated using the principal components given in Table 4; bottom: spectrum at a spin rate of 1.25 kHz.

ne)$_4$SiH$_2$]$^{2+}$, [(3-methylpyridine)$_4$SiH$_2$]$^{2+}$, [(3,4-dimethylpyridine)$_4$SiH$_2$]$^{2+}$, [(3,5-dimethylpyridine)$_4$SiH$_2$]$^{2+}$ and [(pyridine)$_4$SiH$_2$]$^{2+}$ (chloride and/or bromide salts; octahedral coordination, *trans* H-Si-H, four pyridine N-atoms on equatorial sites).[15–17] Irrespective of the synthesis path described above, single crystals of the hexacoordinate complexes **1a–c** and **1f** were obtained directly upon extraction with $CHCl_3$. The Cl_3C–H→Cl contacts to the chloride ion in complexes **3d** and **3e** (approx. 245 pm) are shorter than the Cl_3C–H→Cl distance between the chloroform molecule in **1c** and the Si-bonded Cl atom (261 pm) because of the anionic charge. The short Si–N bonds in **1c** and the resulting longer Si–Cl bonds, which represent a step on the way to base-supported Si–Cl dissociation and chloride ion formation, can be related to the incorporation of the chloroform molecule in the structure of **1c**.

Measurement and calculation of the ^{29}Si NMR chemical shift tensor: The ^{29}Si NMR chemical shift tensors were determined in order to get a better understanding of the ^{29}Si NMR shielding of these compounds. The principal components, and subsequently the isotropic chemical shift, the span (Ω; anisotropy) and skew (κ) of the tensor were extracted from spinning side-band ^{29}Si CP/MAS spectra according to the Herzfeld–Berger convention.[18,19] The ^{29}Si CP/MAS spectrum of **1e** is given in Figure 8 as an example.

We also calculated the ^{29}Si NMR principal components by the GIAO method based on the geometries of the crystal structures (see Table 4). The observed and calculated spans are quite large in comparison with those for other hexacoordinate Si complexes. Figure 9 shows the orientation of the principal components in the molecular structure of compound **1b**.

Table 4. ^{29}Si MAS NMR spectroscopic data and results of GIAO calculations (B3LYP/6-311+G(2d,p)) of the ^{29}Si NMR shifts of compounds **1a–f** and **2**.

Molecule		δ_{iso}[a]	δ_{11}	δ_{22}	δ_{33}	Ω[b]	κ[b]
1a	exp	−145.4	−47.5	−185.9	−202.8	155.3	−0.8
	calc	−159.8	−74.3	−187.7	−217.4	143.1	−0.6
1b	exp	−147.2	−51.0	−187.3	−203.3	152.2	−0.8
	calc	−165.0	−87.4	−190.5	−217.1	129.7	−0.6
1c	exp	−152.1	−75.7	−180.9	−199.7	124.0	−0.7
	calc	−173.1	−106.4	−195.0	−217.8	111.3	−0.6
1d	exp	−148.8	−51.8	−185.1	−209.5	157.7	−0.7
	calc	−164.3	−83.4	−191.5	−217.9	134.5	−0.6
1e	exp	−152.3	−66.1	−185.1	−205.7	139.6	−0.7
	calc	−166.3	−95.2	−186.7	−216.9	121.6	−0.5
1f	exp	−149.6	−49.5	−189.3	−210.0	160.5	−0.7
	calc	−165.9	−83.7	−192.3	−221.6	138.0	−0.6
2	exp	−149.1	−49.0	−187.8	−210.5	161.5	−0.7
	calc	−160.4	−74.0	−184.9	−222.4	148.4	−0.5

[a] Chemical shift in the solid state. [b] Herzfeld–Berger convention, $\Omega=\delta_{11}-\delta_{33}$, $\kappa=3(\delta_{22}-\delta_{iso})/\Omega$.

The principal components of the investigated compounds **1** point along the E-Si-E (E = Cl, H, N) bond axes, with the highest shielding being observed in the direction of the Si–N bonds (δ_{33}) and the lowest shielding along the Si–Cl bonds (δ_{11}). Both the calculated and the experimental values of the skew range between −0.5 and −0.9, which means that the shielding in the direction of the Si–H bonds (δ_{22}) is only slightly smaller than δ_{33}. The silicon nucleus is therefore strongly shielded in the direction of the hydrogen and pyridine substituents and less shielded in the direction of the Si–Cl bonds. The span decreases for both the experimental

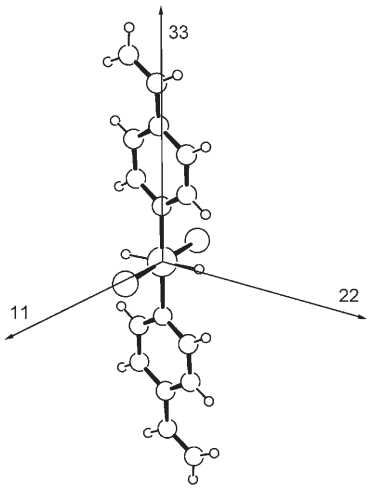

Figure 9. Orientation of the principal shielding tensor components in **1b**.

and the calculated tensors nearly in the same order: **1f** > **1d** > **1a** > **1b** > **1e** > **1c** (exp. values). Compound **1c** has a noticeably smaller span than the other complexes **1**, which we attribute to the quinoid-like resonance structure of this derivative (see Scheme 2). The differences in the spans of the complexes are due to changes in both δ_{11} and δ_{33}, although δ_{11} seems to have a higher contribution to Ω. The pyrazine derivative has the highest span and a skew of −0.7 as a result of two directions with higher shielding, similar to the pyridine derivatives.

There are some deviations between the experimental and calculated tensor components, with the calculated span being smaller than the experimental one. The highest deviation between calculated and measured isotropic shift values (δ_{iso}) is 22 ppm. A comparison between the calculated and experimental principal components shows a good accordance for δ_{22}, but significant deviations for δ_{33} and especially δ_{11}, the components which are nearly perpendicular to the Si–H bonds. It has been shown previously[20,21] that silicon-bound hydrogen atoms cause inaccuracies in ^{29}Si NMR shift calculations, and this problem has not yet been solved theoretically.

Density functional theory (DFT) calculations: Quantum chemical calculations were performed to obtain a better insight into the bonding features of the compounds under investigation. Topological analysis of the electron-density distribution is a powerful tool for that purpose, and this analysis can be carried out using the atoms-in-molecules theory (AIM) developed by Bader and others.[22–25] This method partitions the electron density of a molecule ρ(r) into individual non-overlapping atomic fragments by rigorously defined interatomic surfaces.[23]

The bond critical points (BCPs) between the atoms of the molecules **1a–f** and **2** represent the topology one would expect for a classical Lewis structure. Figure 10 shows one such example. A more detailed analysis is only possible, however, by looking at the properties of the electron density

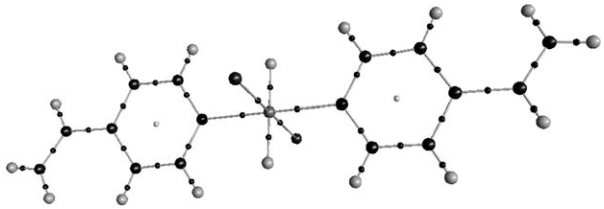

Figure 10. Molecular representation of **1b** showing the BCPs (small black dots on the bond paths). The atomic spheres are drawn with arbitrary radii.

at the BCPs. Table 5 shows these properties for the BCPs that connect the silicon atoms with their surrounding ligands and substituents in the compounds under investigation.

Table 5. Electron density (ρ), Laplacian ($\nabla^2\rho$) and bond ellipticity (ε) at selected BCPs in **1a–f** and **2**.

	ρ [e Å^{-3}]	$\nabla^2\rho$ [e Å^{-5}]	ε
Si–H			
1a	1.035	5.995	0.029
1b	0.983	4.802	0.032
1c	0.920	3.424	0.036
1d	1.024	5.790	0.029
1e	1.027	5.860	0.030
1f	0.998	5.154	0.030
2	1.019	5.590	0.029
Si–Cl			
1a	0.431	1.320	0.440
1b	0.428	1.288	0.418
1c	0.413	1.128	0.447
1d	0.433	1.427	0.431
1e	0.432	1.388	0.419
1f	0.438	1.463	0.413
2	0.443	1.432	0.416
Si–N			
1a	0.513	4.927	0.194
1b	0.530	5.120	0.165
1c	0.563	5.561	0.129
1d	0.519	4.946	0.185
1e	0.528	5.057	0.176
1f	0.522	4.990	0.175
2	0.508	4.877	0.194

The graphical representation of the Laplacian $\nabla^2\rho$ and the electron density maps (ρ(r)) in Figure 11 shows that there is very low electron density at the BCPs between Si and Cl and slightly positive values of the Laplacian, which suggests a predominantly ionic interaction. The graphical representation of the Laplacian, with its nearly spherical charge concentration around the chlorine atom, confirms this assumption. The remarkable bond ellipticity at the BCPs between Si and Cl hints at some π-donation from lone pairs at chlorine atoms into unoccupied orbitals at silicon. However, if we classify the interaction between Si and Cl as ionic, it would be unreasonable to designate a "partial double-bond character" to these bonds. A closer look at

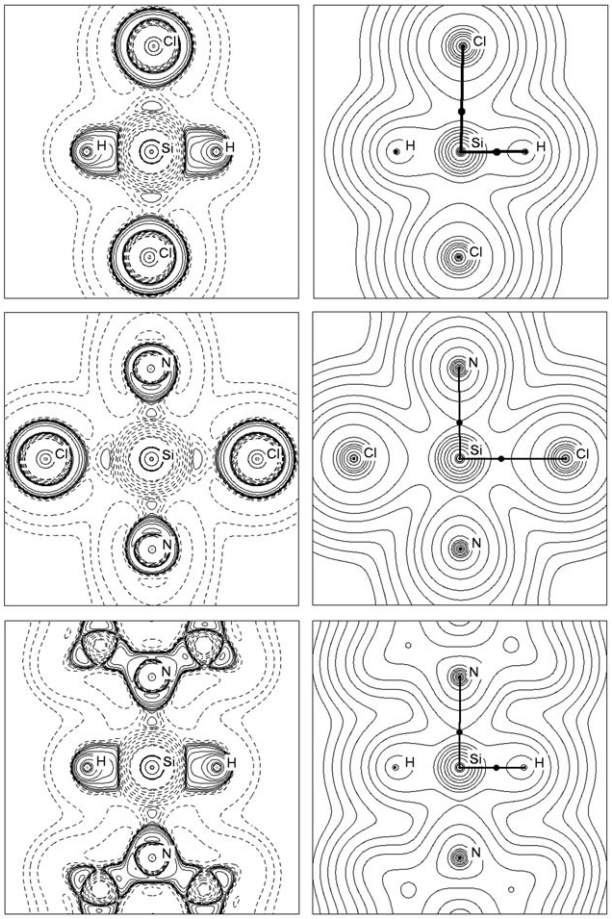

Figure 11. Representation of the topological properties of **1b** in different planes: SiH_2Cl_2 (top), SiN_2Cl_2 (middle) and SiH_2N_2 (bottom). Left column: Laplacian of the electron density. Positive values of $\nabla^2\rho$ are drawn with dashed lines and represent regions of charge depletion; negative values of $\nabla^2\rho$ are drawn with solid lines and represent regions of charge concentration. Right column: electron density. Selected bond paths and bond critical points are included in the figures. The contour values for both representations in atomic units are: 0.001, 0.002, 0.004, 0.008, 0.02, 0.04, 0.08, 0.2, 0.4, 0.8, 2, 4, 8, 20, 40, 80, 200, 400 and 800.

electron density distribution at the BCP between Si and Cl shows that the electronic charge is preferentially accumulated in the $SiCl_2H_2$ plane (see Figure 12). The charge density of the hydrogen atom is polarised towards the positively charged silicon atom, which leads to a notable charge concentration at the Si–H bond axis and higher electron density at the BCPs. This can be interpreted in terms of a polar covalent bond, although the positive value of the Laplacian would suggest otherwise. A closer examination of the position of the BCP in this case shows that this point is located close to the nodal surface in $\nabla^2\rho$, where the atomic basins of Si and H exhibit an opposite behaviour with respect to the sign of the Laplacian of ρ. Such interactions have been classified as "intermediate interactions" and range from closed-shell to shared interactions.[26]

The Si–N bonds are polar with considerable ionic contribution to the bonding, with similar values for ρ as for the Si–Cl bonds. The main differences between these two bond

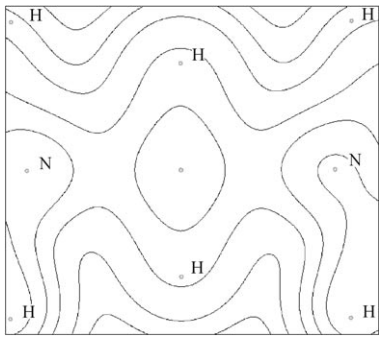

Figure 12. Contour map of ρ at the BCP between Si and Cl. The plane of the plot is perpendicular to the Si–Cl axis and shows the elliptical deformation of the electron density into the $SiCl_2H_2$ plane.

types are the higher positive value of the Laplacian (see Table 6) and the small but clearly visible charge concentration at the nitrogen atom in the former, which reflects the donor–acceptor interaction between N and Si. The results of the AIM analysis suggest that the canonical form **C** is the best description of the bonding features between silicon and the surrounding ligands and substituents in compounds of type **1** (Scheme 4). Similar conclusions have been drawn from experimental and theoretical charge-density studies in hexacoordinate silicon complexes with an $[SiO_2N_2F_2]$ coordination framework.[27]

An alternative description of the chemical bonding between the silicon atom and its surrounding atoms is provided by the natural bond orbital (NBO) analysis. This method, developed by Weinhold et al.,[28] uses the one-electron matrix as a starting point to find the best Lewis structure of the molecule. Bond polarisations, hybridisations of the atoms, partial charges and the electron configuration of the atoms can all be calculated by this method, which has been described previously in detail.[28–30]

The four valence structures of **1b** depicted in Scheme 4 were investigated by the NBO method. The valence structure with six covalent bonds from the silicon atom, which corresponds to an sp^3d^2 hybridisation (**A**), has 96.31% Lewis character, in other words the electrons are located to a degree of 96.31% in localised hybrid orbitals. The other valence structure with four covalent bonds to hydrogen and chlorine, which has an sp^2d configuration at the central silicon atom, has 97.56% Lewis character (**B**). The remaining valence structures with covalent bonds to the hydrogen and the nitrogen atoms (**C**) and solely to the hydrogen atoms (**D**) have 97.40% and 97.34% Lewis character, respectively. Thus, the valence structures **B**–**D** represent similarly good descriptions for this type of compound. Further valence structures with ionic Si–H interactions are imaginable but, due to the lower bond polarity of these bonds, such valence structures are less probable and will not be considered here.

All four valence structures are discussed in the following paragraphs. Structure **A** has a large non-Lewis character (3.69%, 5.97 e), which makes this structure less probable. The Si hybridisation can be denoted as sp^3d^2 with ideal par-

Table 6. Results of the NBO analysis for **1b** and H_2SiCl_2.[a]

Molecule/bond	Occ.	% Si	AO of Si [%]			AO of E [%]		
			s	p	d	s	p	d
H_2SiCl_2								
Si–Cl	1.99	26.71	21.98	75.67	2.35	20.19	79.33	0.48
Si–H	1.97	42.75	28.15	70.84	1.02	99.88	0.12	–
1b (valence structure **A**)								
Si–Cl	1.88	15.86	15.69	50.0	34.31	20.61	79.25	0.14
Si–H	1.79	32.61	23.58	50.0	26.42	99.33	0.67	–
Si–N	1.90	9.91	16.16	50.0	33.84	32.71	67.28	0.02
1b (valence structure **B**)								
Si–Cl	1.90	16.92	20.73	50.0	29.27	20.59	79.27	0.14
Si–H	1.87	35.76	33.94	50.0	16.06	99.33	0.67	–
1b (valence structure **C**)								
Si–N	1.91	10.64	21.37	50.0	28.63	32.70	67.28	0.02
Si–H	1.84	35.01	29.42	50.0	20.58	99.33	0.67	
1b (valence structure **D**)								
Si–H	1.98	40.62	49.64	50.0	0.36	99.33	0.67	–

[a] Occ: occupancy of the bond; % Si: share of the atomic orbitals of Si in the molecule orbital; AO: atomic orbitals that contribute to the bonds

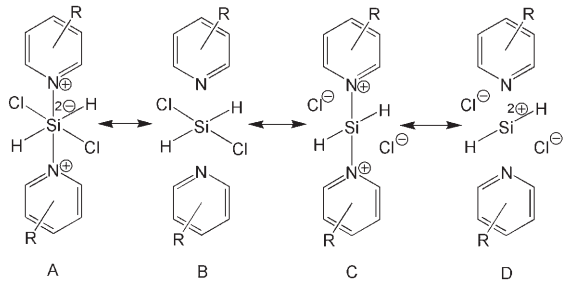

Scheme 4. Possible Lewis structures for compounds of type **1**.

tition of the hybrid orbitals of 16.7% s, 50% p and 33.3% d. The only major deviation from this ideal state is observed for the Si–H bonds, which have 23.58% s-character at Si. The shorter Si–H bond has a higher s-character than the Si–Cl and Si–N bonds. All three bond types (Si–Cl, Si–H, Si–N) are occupied by nearly two electrons. Information about the bond polarity can be obtained from the percentage of Si in the bond orbital. A non-polar covalent bond has percentages close to 50% for both atoms, whereas a share of 32.61% Si for the Si–H bond indicates a polar bond where the electron density is shifted towards the H atom. The Si–Cl bond, which has an Si contribution of 15.86%, is even more polar. The highest polarity in **A** is observed for the Si–N interaction (90.09% N and 9.91% Si). This interaction is a borderline case which should be considered as a donor–acceptor interaction.

The Si-atom hybridisation in **B** can be categorised as sp^2d. The combination of s, p_x, p_y and $d_{x^2-y^2}$ orbitals produces hybrid orbitals in the *xy* plane. Ideal sp^2d-hybridisation involves 25% s, 50% p and 25% d character. There are deviations from the ideal bonding state in this structure since there is a higher proportion of s character (33.94%) in the Si–H bond (Table 6) and a higher proportion of d character (29.27%) in the Si–Cl bond. These differences can be correlated with the different bond lengths, as discussed above. The longer Si–Cl bond requires spatially more extended d-orbitals at Si than the short Si–H bond. Nevertheless, sp^2d hybridisation represents a suitable bonding model for this Lewis structure. The Si–Cl bonds are strongly polarised toward the Cl atom (83.08%), although the Si–H bonds are less polarised (64.24% H). The p_z orbital at Si is occupied by only 0.40 e and is suitable for donor–acceptor interactions with the lone pairs of the N atoms, which are occupied by 1.73 e. The second-order perturbation theory analysis gives a stabilizing effect of 502 kJ mol^{-1} for each N–Si interaction, although this value must not be interpreted as the bond energy.

The hybridisation of the silicon atom in structure **C** is also sp^2d. The combination of s, p_x, p_z and d_{z^2} orbitals produces four hybrid orbitals in the *xz* plane. The Si–N bonds are strongly polarised toward the N atom (89.36%) and the Si–H bonds are less polarised (64.99% H). The p_y orbital at Si is occupied by 0.58 e and this orbital is suitable for donor–acceptor interactions with the lone pairs of the Cl atoms, which are occupied by 1.61 e. The second-order perturbation theory analysis gives a stabilizing effect of 847 kJ mol^{-1} for each Cl–Si interaction.

The hybridisation of the silicon atom in structure **D** can be categorised as sp. This is indeed found for these bonds, with 49.64% s, 50% p and a minor share of d-character in the hybrid orbitals at Si. The Si–H bonds in this valence structure are only weakly polarised (40.62% Si). All other orbital interactions in this structure must be treated with second-order perturbation theory. The N–Si interaction has already been discussed in the previous section, and each interaction between Cl and Si gives a stabilizing effect of 864 kJ mol^{-1} if it is treated as a perturbation of this valence structure.

The natural charges of **1b** and of selected reference molecules are shown in Table 7. The charge of the silicon atom increases from 1.02 to 1.17 upon complex formation. A simi-

Table 7. Natural charges of the atoms in **1b** and selected reference molecules.

Molecule	Atom	Natural charge
pyridine	N	−0.46
H_2SiCl_2	Si	1.02
	Cl	−0.35
	H	−0.16
1b	Si	1.17
	Cl	−0.55
	H	−0.24
	N	−0.53

lar effect has already been discussed for antimony, tin and silicon complexes.[5,8,31] The negative charge on the pyridine nitrogen atom also increases upon complex formation. Furthermore, the chlorine and hydrogen atoms also bear higher negative charges in complex **1b** than in H_2SiCl_2. These changes in the charge distribution are evidence for a bonding situation in the complex that involves generally more polar bonds than in the starting molecule H_2SiCl_2. This assumption is confirmed by the bond polarities shown in Table 6. The Si–Cl bond has 26.71 % Si character in H_2SiCl_2, and this value decreases to 15.86 % and 16.92 % for the valence structures **A** and **B**, respectively. A similar effect is observed for the Si–H bond.

Conclusion

Hexacoordinate dichlorosilane/pyridine adducts have been synthesised in various aprotic solvents by the direct reaction of H_2SiCl_2 with pyridine. The first example of an H_2SiCl_2·2 Rpy compound bearing non-coplanar pyridine rings has been found, although a coplanar arrangement of the pyridine ligands seems to be the most typical conformation in the solid state. Quantum chemical analysis demonstrates that both coordination modes may be favourable. Some of these pyridine adducts (those bearing 4-methyl- and 4-ethylpyridine) have been shown to undergo ligand redistribution when extracted with hot chloroform to yield the hexacoordinate siliconium salts $[H_2Si(RPy)_4]Cl_2$, the anion of which is stabilised by chloroform molecules.

The ^{29}Si CP/MAS NMR spectra of the adducts H_2SiCl_2·2 Rpy reveal large spans for the shielding tensors of their octahedrally coordinated silicon nuclei, and GIAO calculations have provided an insight into the directions of the principal components [(11), (22) and (33)] of the shielding tensors, which point almost along the Cl-Si-Cl, H-Si-H and N-Si-N axes, respectively. The highest shielding is observed in the direction of the Si–H and Si–N bonds, and the shielding is considerably lower in the direction of the Si–Cl bonds. Quantitative descriptions of those shielding tensors, however, are difficult due to general problems with the modelling of H–Si bond influences on ^{29}Si NMR properties, which have not yet been overcome.

Four possible valence structures **A**–**D** have been investigated with the NBO method, with the valence structures **B**, **C** and **D** being equally good descriptions of the bonding situation. The NBO analysis reveals that these structures contain polar covalent Si–H bonds, strong polar Si–Cl bonds, and that the highest bond polarisation is observed for the Si–N interaction, which therefore has to be considered as a donor–acceptor interaction. Analysis of the topological properties of the electron density distribution (AIM) suggests that the Lewis structure **C** is the best description for the bonding situation in molecules of the type H_2SiCl_2·2 Rpy.

Experimental Section

Caution: Handling of dichlorosilane is not trivial due to its low boiling point of 8.4 °C and oxidative and hydrolytic sensitivity. All reactions were carried out under dry argon using Schlenk techniques. Solvents were dried and purified by standard methods. CP/MAS NMR spectra were recorded with a Bruker Avance 400 MHz WB spectrometer by using a 7-mm probehead with zirconia rotors and KelF inserts operating at 400.23, 100.61 and 79.51 MHz for ^{1}H, ^{13}C and ^{29}Si, respectively. Chemical shifts are reported in ppm relative to TMS. Raman spectra were recorded with a Bruker RFS 100/S instrument equipped with an Nd/YAG Laser. X-ray single crystal structure analyses were carried out with a Bruker Nonius X8 APEX2 CCD diffractometer. Elemental analysis (determination of the chlorine content of product **1c**) was performed by hydrolysis of 0.15 g of **1c** in 100 mL of dilute sodium hydroxide solution followed by chloride quantification by ion chromatography (Dionex, ICS-2000; eluent: 22 mM KOH; column: AS11 HC, electrical conductivity measurement).

The structures were solved by direct methods and refined by full-matrix least-squares methods. All non-hydrogen atoms were refined anisotropically. Carbon-bonded hydrogen atoms were placed in idealised positions and refined isotropically (riding model). Si-bonded hydrogen atoms were found by analysis of the residual electron density and refined without bond length restraints. Structure solution and refinement of F^2 against all reflections were carried out with the software SHELXS-97 and SHELXL-97 (G. M. Sheldrick, Universität Göttingen (1986–1997)). Structure determination and refinement data for the crystal structures presented in this paper are summarised in Tables 8, 9 and 10. CCDC 621840 (**1a**), 621841 (**1b**), 621839 (**1c**), 634403 (**1d**), 621844 (**1e**), 621843 (**1f**), 621845 (**2**), 621846 (**3d**) and 621842 (**3e**) contain the supplementary crystallographic data for this paper. These data can be obtained free of charge from the Cambridge Crystallographic Data Centre via www.ccdc.cam.ac.uk/data_request/cif.

The Quantum chemical calculations were carried out using the GAUSSIAN 03 program suite.[32] The solid-state geometries obtained from X-ray structure analyses were used for the calculations without further optimisation. The calculations were performed at the density functional theory level (DFT), using Becke's three-parameter hybrid exchange functional and the correlation functional of Lee, Yang and Parr (B3LYP),[33,34] with the 6-311+G(2d,p) basis set for all atoms.[35–37]

The AIM analyses[22] were performed at the B3LYP/6-311+G(2d,p) level with the geometries obtained from the X-ray structure analyses.

The wavefunction files for the AIM analysis were generated in Cartesian coordinates with a basis set containing 6d functions (option "6D 10F" in Gaussian 03). The electron-density topology was analysed by using the programs AIM2000[38] and Xaim.[39]

The NBO analyses were performed with NBO 3.0.[28] The different valence structures **A**–**D** were generated with the "CHOOSE" option in the NBO programme.

Relaxed potential energy surface (PES) scans were performed with the Opt=ModRedundant utility in Gaussian 03 with B3LYP/6-31G(d). This option includes the specification of redundant internal coordinates. In these cases, a specific torsion angle was changed in 5° steps. The geometry of the molecule was completely optimised in every step whilst restricting only the torsion angle to the specified value. This method allows access to a defined section of the potential energy surface.

The principal components of the NMR shielding tensor were extracted from the spectra using the HB-MAS program (D. Fenzke, Universität Leipzig 1989).

NMR shielding tensors were calculated by the Gauge-Independent Atomic Orbital method (GIAO)[40] at the B3LYP/6-311+G(2d,p) level of theory with the geometries obtained from the X-ray structure analyses. Calculated absolute shielding values were converted to relative shifts (δ) by calculating the shielding of tetramethylsilane at the same level of theory.

H_2SiCl_2 (Degussa), 4-methylpyridine (Alfa Aesar), 4-ethylpyridine (Merck), 3-bromopyridine (ABCR), 4-*tert*-butylpyridine (Fluka), 4-vinyl-

Table 8. Crystal data and structure refinement for **1a**, **1b** and **1c**·2 $CHCl_3$.

	1a	**1b**	**1c**·2 $CHCl_3$
empirical formula	$C_{10}H_{10}Br_2Cl_2N_2Si$	$C_{14}H_{16}Cl_2N_2Si$	$C_{16}H_{24}Cl_8N_4Si$
formula weight	417.01	311.28	584.08
T [K]	93(2)	93(2)	93(2)
λ [Å]	0.71073	0.71073	0.71073
crystal system	monoclinic	monoclinic	triclinic
space group	$C2/c$	$P2_1/n$	$P\bar{1}$
a [Å]	18.8249(8)	7.0686(5)	7.1762(10)
b [Å]	5.6038(2)	8.1304(6)	8.9359(12)
c [Å]	14.6931(6)	13.5961(10)	10.6509(15)
α [°]	90	90	113.895(6)
β [°]	117.762(2)	101.653(2)	93.773(6)
γ [°]	90	90	94.148(6)
V [Å^3]	1371.57(10)	765.27(10)	619.42(15)
Z	4	2	1
ρ_{calc} [Mg m^{-3}]	2.019	1.351	1.566
absorption coefficient [mm^{-1}]	6.365	0.490	0.970
$F(000)$	808	324	298
crystal size [mm^3]	$0.67\times0.12\times0.06$	$0.30\times0.22\times0.05$	$0.28\times0.10\times0.04$
θ range for data collection [°]	3.84–36.99	3.58–27.50	2.86–26.99
index ranges	$-29\le h\le31$, $-9\le k\le9$, $-24\le l\le23$	$-9\le h\le9$, $-9\le k\le10$, $-17\le l\le17$	$-9\le h\le9$, $-11\le k\le10$, $0\le l\le13$
reflections collected	11221	5584	6384
independent reflections, R_{int}	3485, 0.0222	1744, 0.0336	2644, 0.0308
completeness to θ_{max} [%]	99.5	99.8	98.7
absorption correction	semiempirical	semiempirical	semiempirical
max./min. transmission	0.6803/0.1524	0.9759/0.8155	0.9622/0.7004
data/restraints/parameters	3485/0/83	1744/0/92	4086/0/137
final R indices [$I>2\sigma(I)$]	$R_1=0.0202$, $wR_2=0.0496$	$R_1=0.0304$, $wR_2=0.0644$	$R_1=0.0489$, $wR_2=0.0962$
R indices (all data)	$R_1=0.0286$, $wR_2=0.0513$	$R_1=0.0477$, $wR_2=0.0683$	$R_1=0.0926$, $wR_2=0.1047$
goodness-of-fit on F^2	1.045	0.998	0.882
largest diff. peak and hole [e Å^{-3}]	1.175, −1.031	0.292, −0.196	0.582, −0.435

Table 9. Crystal data and structure refinement for **1d**, **1e** and **1f**.

	1d	**1e**	**1f**
empirical formula	$C_{12}H_{16}Cl_2N_2Si$	$C_{14}H_{20}Cl_2N_2Si$	$C_{18}H_{28}Cl_2N_2Si$
formula weight	287.26	315.31	371.41
T [K]	90(2)	90(2)	153(2)
λ [Å]	0.71073	0.71073	0.71073
crystal system	monoclinic	monoclinic	monoclinic
space group	$P2_1/n$	$C2/c$	$C2/c$
a [Å]	5.9012(7)	11.8426(4)	19.6243(7)
b [Å]	8.0579(9)	9.2001(3)	8.0608(2)
c [Å]	14.8296(18)	14.3452(4)	13.7150(4)
α [°]	90	90	90
β [°]	105.374(6)	99.199(2)	111.674(2)
γ [°]	90	90	90
V [Å^3]	679.93(14)	1542.85(8)	2016.16(11)
Z	2	4	4
ρ [Mg m^{-3}]	1.403	1.357	1.224
absorption coefficient [mm^{-1}]	0.545	0.487	0.383
$F(000)$	300	664	792
crystal size [mm^3]	$0.65\times0.38\times0.25$	$0.50\times0.40\times0.25$	$0.43\times0.35\times0.02$
θ range for data collection [°]	2.82–34.00	2.82–48.00	2.23–30.00
index ranges	$-9\le h\le9$, $-12\le k\le12$, $-23\le l\le22$	$-24\le h\le24$, $-11\le k\le19$, $-29\le l\le29$	$-27\le h\le27$, $-11\le k\le11$, $-18\le l\le19$
reflections collected	15534	24634	15622
independent reflections, R_{int}	2691, 0.0512	7361, 0.0242	2943, 0.0298
completeness to θ_{max} [%]	96.9	99.7	100.0
absorption correction	semiempirical	semiempirical	semiempirical
max./min. transmission	0.8758/0.7130	0.8879/0.7952	0.9924/0.9072
data/restraints/parameters	2691/0/84	7361/0/92	2943/0/110
final R indices [$I>2\sigma(I)$]	$R_1=0.0536$, $wR_2=0.1736$	$R_1=0.0308$, $wR_2=0.0842$	$R_1=0.0328$, $wR_2=0.0774$
R indices (all data)	$R_1=0.0562$, $wR_2=0.1751$	$R_1=0.0490$, $wR_2=0.0899$	$R_1=0.0538$, $wR_2=0.0839$
goodness-of-fit on F^2	1.161	1.046	1.039
largest diff. peak and hole [e Å^{-3}]	1.167, −0.669	0.659, −0.328	0.358, −0.236

Table 10. Crystal data and structure refinement for **2**, **3d**·6 $CHCl_3$ and **3e**·6 $CHCl_3$.

	2	**3d**·6 $CHCl_3$	**3e**·6 $CHCl_3$
empirical formula	$C_8H_{10}Cl_2N_4Si$	$C_{30}H_{36}Cl_{20}N_4Si$	$C_{34}H_{44}Cl_{20}N_4Si$
formula weight	261.19	1189.72	1245.82
T [K]	90(2)	90(2)	203(2)
λ [Å]	0.71073	0.71073	0.71073
crystal system	monoclinic	triclinic	triclinic
space group	$P2_1/c$	$P\bar{1}$	$P\bar{1}$
a [Å]	7.29226(2)	9.3107(3)	9.7197(4)
b [Å]	8.5929(2)	11.0529(4)	11.0942(5)
c [Å]	9.5100(3)	12.7008(4)	13.3461(7)
α [°]	90	93.209(2)	90.778(2)
β [°]	107.6629(16)	100.801(2)	101.771(2)
γ [°]	90	97.862(2)	96.028(1)
V [Å^3]	567.85(3)	1267.34(7)	1400.18(11)
Z	2	1	1
ρ [Mg m^{-3}]	1.528	1.559	1.477
absorption coefficient [mm^{-1}]	0.649	1.130	1.026
F(000)	268	598	630
crystal size [mm^3]	0.23 × 0.17 × 0.08	0.75 × 0.50 × 0.40	0.35 × 0.25 × 0.20
θ range for data collection [°]	2.93–34.00	2.25–35.00	2.37–28.00
index ranges	$-11 \le h \le 11$, $-13 \le k \le 13$, $-14 \le l \le 14$	$-15 \le h \le 15$, $-17 \le k \le 17$, $-20 \le l \le 20$	$-11 \le h \le 12$, $-14 \le k \le 14$, $-17 \le l \le 17$
reflections collected	17761	57513	18146
independent reflections, R_{int}	2317, 0.0312	11138, 0.0245	6724, 0.0208
completeness to θ_{max} [%]	100.0	99.9	99.4
absorption correction	semiempirical	semiempirical	semiempirical
max./min. transmission	0.9499, 0.8549	0.6343, 0.566	0.8211, 0.7554
data/restraints/parameters	2317/0/74	11138/0/256	6724/68/358
final R indices [$I > 2\sigma(I)$]	$R_1 = 0.0406$, $wR_2 = 0.0732$	$R_1 = 0.0334$, $wR_2 = 0.0823$	$R_1 = 0.0476$, $wR_2 = 0.1250$
R indices (all data)	$R_1 = 0.0734$, $wR_2 = 0.0793$	$R_1 = 0.0426$, $wR_2 = 0.0862$	$R_1 = 0.0660$, $wR_2 = 0.1327$
goodness-of-fit on F^2	0.804	1.085	1.083
largest diff. peak and hole [e Å^{-3}]	0.536, −0.454	1.412, −1.203	0.457, −0.411

pyridine (Aldrich), 4-(dimethylamino)pyridine (Fluka), pyridine (Riedel de Haen) and pyrazine (Fluka) were obtained commercially. Liquid substituted and unsubstituted pyridines were heated over CaH_2 for several hours and then distilled and stored over 3-Å molecular sieves. Solid compounds were dried under vacuum for several hours. Dichlorosilane was used as supplied (Degussa 99.999 %) and employed as a 40 vol % solution for ease of handling. Dichlorosilane (4 mL) was condensed in a flask and the desired solvent (6 mL) was added.

Compounds **1a–f** and **2** were synthesised as follows. Dichlorosilane (5 mmol) was dissolved in toluene (30 mL) at −78 °C and the pyridine base (10 mmol) was added dropwise. The products precipitated as colourless solids. The suspension was stirred for one hour at this temperature and than slowly heated to room temperature. The resultant white precipitate was filtered off, washed with toluene and dried under vacuum.

Dichlorodihydridodipyridinesilane: $H_2SiCl_2(NC_5H_5)_2$ has been obtained previously by dismutation of $HSiCl_3$ in the presence of pyridine[3] or by decomposition of $N(CH_3)(SiHCl_2)_2$ also in the presence of pyridine (see introduction). We, however, synthesised the compound directly from H_2SiCl_2 and pyridine as described above. Yield: 1.26 g (4.90 mmol; 98 %), ^{29}Si CP/MAS NMR (ν_{spin} = 5 kHz): δ_{iso} = −145.3 ppm; ^{13}C CP/MAS NMR (ν_{spin} = 5 kHz): δ_{iso} = 126.9, 141.2, 144.5 ppm; Raman: $\tilde{\nu}$ = 650 (m), 923 (w), 1020 (s), 1065 (w), 1153 (w), 1205 (m), 1262 (w), [ν(SiH)] 2075 (m), 2515 (w), 2928 (w), 2968 (w), 3008 (w), 3034 (w), 3063 (m), 3075 (s), 3149 cm^{-1} (m).

Di(3-bromopyridine)dichlorodihydridosilane ***(1a)***: Yield: 1.43 g (3.45 mmol; 69 %), ^{29}Si CP/MAS NMR (ν_{spin} = 5 kHz): δ_{iso} = −145.2 ppm; ^{13}C CP/MAS NMR (ν_{spin} = 4 kHz): δ_{iso} = 111.4, 117.1, 128.8, 143.6 ppm; Raman: $\tilde{\nu}$ = 251 (m), 300 (m), 334 (m), 487 (w), 655 (w), 723 (w), 825 (w), 928 (w), 1034 (s), 1062 (w), 1101 (w), 1126 (w), 1192 (w), 1253 (w), 1317 (w) 1417 (w), 1468 (w), 1563 (w), 1603 (m), [ν(Si-H)] 2103 (w), 2501 (w), 2929 (w), 3011 (w), 3064 (s), 3089 (w), 3129 (w), 3203 cm^{-1} (w). Single crystals of **1a** were obtained by extraction with boiling $CHCl_3$.

Dichlorodihydridodi(4-vinylpyridine)silane ***(1b)***: Yield: 1.40 g (4.53 mmol; 91 %), ^{29}Si CP/MAS NMR (ν_{spin} = 5 kHz): δ_{iso} = −147.2 ppm; ^{13}C CP/MAS NMR (ν_{spin} = 5 kHz): δ_{iso} = 123.8, 127.0, 134.7, 141.8, 151.9 ppm; Raman: $\tilde{\nu}$ = 249 (m), 289 (w), 464 (w), 666 (w), 807 (w), 856 (w), 954 (w), 1002 (w), 1028 (m), 1045 (m), 1073 (m), 1211 (m), 1262 (w), 1305 (w), 1338 (w), 1421 (m), 1438 (m), 1506 (w), 1551 (w), 1621 (s), 1632 (s), [ν(Si-H)] 2078 (w), 2514 (w), 2919 (w), 2978 (w), 2990 (w), 3072 cm^{-1} (m). Single crystals of **1b** were obtained by extraction with boiling $CHCl_3$.

Dichlorobis[4-(dimethylamino)pyridine]dihydridosilane ***(1c)***: THF was used for the synthesis of **1c** instead of toluene. Yield: 1.59 g (4.63 mmol; 93 %); ^{29}Si CP/MAS NMR (ν_{spin} = 5 kHz): δ_{iso} = −151.8 ppm; ^{13}C CP/MAS NMR (ν_{spin} = 4 kHz): δ_{iso} = 38.9, 39.6, 107.2, 141.8, 143.4, 156.1 ppm; Raman: Dual bands for [ν(SiH)] at about 2050 cm^{-1}; elemental analysis calcd (%) for $C_{14}H_{22}Cl_2N_4Si$ (344.10): Cl 20.6; found: Cl 18.9. Single crystals of **1c** were obtained by extraction with boiling $CHCl_3$.

Dichlorodihydridodi(4-methylpyridine)silane ***(1d)***: Yield: 1.32 g (4.63 mmol; 93 %); ^{29}Si CP/MAS NMR (ν_{spin} = 5 kHz): δ_{iso} = −148.8 ppm; ^{13}C CP/MAS NMR (ν_{spin} = 6.5 kHz): δ_{iso} = 23.1, 128.1, 140.4, 144.7, 157.3 ppm; Raman: $\tilde{\nu}$ = 256 (m), 292 (m), 364 (w), 555 (w), 668 (m), 878 (m), 941 (w), 1005 (w), 1042 (m), 1067 (m), 1204 (m), 1226 (m), 1261 (w), 1324 (w) 1377 (w), 1563 (w), 1626 (m), [ν(Si-H)] 2080 (w), 2515 (w), 2919 (s), 2998 (w), 3068 cm^{-1} (s). Single crystals of **1d** were obtained by extraction with boiling CH_3CN.

Dichlorodi(4-ethylpyridine)dihydridosilane ***(1e)***: Yield: 1.53 g (4.89 mmol; 98 %); ^{29}Si CP/MAS NMR (ν_{spin} = 5 kHz): δ_{iso} = −152.2 ppm; ^{13}C CP/MAS NMR (ν_{spin} = 6.5 kHz): δ_{iso} = 17.4, 29.1, 128.0, 143.2, 162.5 ppm; Raman: $\tilde{\nu}$ = 248 (m), 332 (w), 400 (w), 526 (w), 585 (w), 650 (w), 666 (m), 745 (w), 799 (m), 970 (w), 1005 (m), 1039 (m), 1064 (m),

1074 (m), 1216 (m), 1279 (w), 1320 (m), 1373 (w), 145 (m), 1461 (m), 1560 (w), 1626 (m), [ν(SiH)] 2061 (m), 2552 (w), 2725 (w), 2874 (m), 2899 (m), 2939 (m), 2972 (m), 2999 (w), 3071 cm^{-1} (s). Single crystals of **1e** were obtained by extraction with boiling CH_3CN.

*Di-(4-tert-butylpyridine)dichlorodihydridosilane (**1f**)*: Yield: 1.76 g (4.77 mmol; 95%); ^{29}Si CP/MAS NMR (ν_{spin} = 5 kHz): δ_{iso} = −149.5 ppm; ^{13}C CP/MAS NMR (ν_{spin} = 6.5 kHz): δ_{iso} = 31.3, 37.3, 124.2, 141.9, 169.7 ppm; Raman: $\tilde{\nu}$ = 252 (m), 337 (w), 370 (w), 397 (w), 550 (w), 667 (m), 734 (m), 753 (m), 844 (w), 928 (m), 940 (w), 1039 (m), 1077 (m), 1129 (m), 1203 (m), 1226 (m), 1274 (m), 1399 (w), 1448 (m), 1466 (m), 1624 (m), [ν(SiH)] 2075 (m), 2529 (w), 2715 (w), 2733 (w), 2865 (w), 2907 (m), 2933 (s), 2954 (m), 2968 (m), 2999 (s), 3077 cm^{-1} (s). Single crystals of **1f** were obtained by extraction with boiling $CHCl_3$.

*Dichlorodihydridodipyrazinesilane (**2**)*: The above-described synthesis route was followed but with a smaller amount of solvent. Thus, dichlorosilane (5 mmol) was condensed in a flask and a solution of 10 mmol of pyrazine in 1 mL of toluene was added. Yield: 1.04 g (3.98 mmol; 80%); ^{29}Si CP/MAS NMR (ν_{spin} = 5 kHz): δ_{iso} = −148.9 ppm; ^{13}C CP/MAS NMR (ν_{spin} = 6.5 kHz): δ_{iso} = 136.0, 149.9 ppm; Raman: $\tilde{\nu}$ = 199 (m), 251 (ms), 471 (w), 649 (w), 680 (w), 696 (m), 920 (w), 939 (w), 1023 (s), 1066 (m), 1119 (w), 1170 (w) 1227 (m), 1421 (w), 1533 (m), 1577 (w), 1606 (m), 2094 (m), 2346 (w), 2900 (w), 2972 (w), 3051 (s), 3063 (s), 3092 cm^{-1} (m).

*Tetrakis(4-ethylpyridino)dihydridosiliconium chloride (**3e**)*: Compound **1e** (1.57 g, 5 mmol) was extracted with 15 mL of boiling $CHCl_3$ and colourless crystals formed within several days after cooling to room temperature. One of these single crystals was selected for X-ray diffraction.

*Dihydridotetrakis(4-methylpyridino)siliconium chloride (**3f**)*: Compound **1f** (1.43 g, 5 mmol) was extracted with 15 mL of boiling $CHCl_3$ and colourless crystals formed within several days after cooling to room temperature. One of these single crystals was selected for X-ray diffraction.

Acknowledgments

We thank Daniela Gerlach, Institut für Anorganische Chemie, TU Bergakademie Freiberg, Leipziger Str. 29, 09596 Freiberg (Germany), for performing the X-ray structure analyses of **1d**. Degussa AG (Rheinfelden, Germany) is acknowledged for a gift of H_2SiCl_2.

[1] U. Wannagat, R. Schwarz, H. Voss, K. G. Knauff, *Z. Anorg. Allg. Chem.* **1954**, *227*, 73–88.
[2] A. B. Burg, *J. Am. Chem. Soc.* **1954**, *76*, 2674–2675.
[3] H. J. Campbell-Ferguson, E. A. V. Ebsworth, *J. Chem. Soc. A* **1966**, 1508–1514.
[4] H. J. Campbell-Ferguson, E. A. V. Ebsworth, *J. Chem. Soc. A* **1967**, 705–712.
[5] K. Hensen, T. Stumpf, M. Bolte, C. Näther, H. Fleischer, *J. Am. Chem. Soc.* **1998**, *120*, 10402–10408.
[6] K. Hensen, M. Kettner, T. Stumpf, M. Bolte, *Z. Naturforsch. Teil B* **2000**, *55*, 901–906.
[7] I. Ignatyev, H. Schaefer III, *J. Phys. Chem. A* **2001**, *105*, 7665–7671.
[8] H. Fleischer, *Eur. J. Inorg. Chem.* **2001**, 393–404.
[9] P. Boudjouk, S. D. Kloos, B. K. Kim, M. Page, D. Thweatt, *J. Chem. Soc. Dalton Trans.* **1998**, 877–879.
[10] J. P. Kintzinger, C. Marsmann, *NMR-Basic Principles and Progress*, Vol 17, Springer Verlag, Berlin, Heidelberg, New York, **1981**.
[11] O. Bechstein, B. Ziemer, D. Hass, S. J. Troyanov, V. B. Rybakov, G. N. Maso, *Z. Anorg. Allg. Chem.* **1990**, *582*, 211–216.
[12] K. Hensen, R. Mayr-Stein, B. Spangenberg, M. Bolte, *Acta Crystallogr. Sect. A* **2000**, *56*, 610–613.
[13] B. Gostevskii, G. Silbert, K. Adear, A. Sivaramakrishna, D. Stalke, S. Deuerlein, N. Kocher, M. Voronkov, I. Kalikhman, D. Kost, *Organometallics* **2005**, *24*, 2913–2920.
[14] D. Kost, V. Kingston, B. Gostevskii, A. Ellern, D. Stalke, B. Walfort, I. Kalikhman, *Organometallics* **2002**, *21*, 2293–2305.
[15] M. Bolte, A. Faber, *Acta Crystallogr. Sect. E* **2001**, *57*, o207–o208.
[16] H. Fleischer, K. Hensen, T. Stumpf, *Chem. Ber.* **1996**, *129*, 765–771.
[17] M. Bolte, K. Hensen, B. Spangenberg, *J. Chem. Crystallogr.* **2000**, *30*, 245–249.
[18] J. Mason, *Solid State Nucl. Magn. Reson.* **1993**, 2, 285–288.
[19] J. Herzfeld, A. E. Berger, *J. Chem. Phys.* **1980**, *73*, 6021–6030.
[20] T. Heine, A. Goursot, G. Seifert, J. Weber, *J. Phys. Chem. A* **2001**, *105*, 620–626.
[21] C. Corminboeuf, T. Heine, J. Weber, *Chem. Phys. Lett.* **2002**, *357*, 1–7.
[22] R. F. W. Bader, *Atoms in Molecules*, Clarendon Press, Oxford, **1994**.
[23] R. J. Gillespie, *J. Chem. Educ.* **2001**, *78*, 1688–1690.
[24] Explanation taken from: R. A. Gillespie, P. L. A. Popelier, *Chemical Bonding and Molecular Geometry*, Oxford University Press, New York, **2001**.
[25] Explanation taken from: N. Kocher, C. Selinka, D. Leusser, D. Kost, I. Kalikhman, D. Stalke, *Z. Anorg. Allg. Chem.* **2004**, *630*, 1777–1793.
[26] R. F. W. Bader, H. Essén, *J. Chem. Phys.* **1984**, *80*, 1943–1960.
[27] N. Kocher, J. Henn, B. Gostevskii, D. Kost, I. Kalikhman, B. Engels, D. Stalke, *J. Am. Chem. Soc.* **2004**, *126*, 5563–5568.
[28] A. E. Reed, L. A. Curtiss, F. Weinhold, *Chem. Rev.* **1988**, *88*, 899–926.
[29] Explanation taken from: J. T. Nelson, W. J. Pietro, *Inorg. Chem.* **1989**, *28*, 544–548.
[30] A. E. Reed, R. B. Weinstock, F. Weinhold, *J. Chem. Phys.* **1985**, *83*, 735–746.
[31] O. K. H. Poleshchuk, E. L. Shevchenko, V. Branchadell, M. Lein, G. Frenking, *Int. J. Quantum Chem.* **2005**, *101*, 869–877.
[32] Gaussian 03, Revision C.02, M. J. Frisch, G. W. Trucks, H. B. Schlegel, G. E. Scuseria, M. A. Robb, J. R. Cheeseman, J. A. Montgomery Jr., T. Vreven, K. N. Kudin, J. C. Burant, J. M. Millam, S. S. Iyengar, J. Tomasi, V. Barone, B. Mennucci, M. Cossi, G. Scalmani, N. Rega, G. A. Petersson, H. Nakatsuji, M. Hada, M. Ehara, K. Toyota, R. Fukuda, J. Hasegawa, M. Ishida, T. Nakajima, Y. Honda, O. Kitao, H. Nakai, M. Klene, X. Li, J. E. Knox, H. P. Hratchian, J. B. Cross, C. Adamo, J. Jaramillo, R. Gomperts, R. E. Stratmann, O. Yazyev, A. J. Austin, R. Cammi, C. Pomelli, J. W. Ochterski, P. Y. Ayala, K. Morokuma, G. A. Voth, P. Salvador, J. J. Dannenberg, V. G. Zakrzewski, S. Dapprich, A. D. Daniels, M. C. Strain, O. Farkas, D. K. Malick, A. D. Rabuck, K. Raghavachari, J. B. Foresman, J. V. Ortiz, Q. Cui, A. G. Baboul, S. Clifford, J. Cioslowski, B. B. Stefanov, G. Liu, A. Liashenko, P. Piskorz, I. Komaromi, R. L. Martin, D. J. Fox, T. Keith, M. A. Al-Laham, C. Y. Peng, A. Nanayakkara, M. Challacombe, P. M. W. Gill, B. Johnson, W. Chen, M. W. Wong, C. Gonzalez, J. A. Pople, Gaussian, Inc., Wallingford CT, **2004**.
[33] A. D. Becke, *J. Chem. Phys.* **1993**, *98*, 5648–5652.
[34] P. J. Stevens, F. J. Devlin, C. F. Chablowski, M. J. Frisch, *J. Phys. Chem.* **1994**, *98*, 11623–11627.
[35] W. J. Hehre, L. Radom, P. v. R. Schleyer, J. A. Pople, *Ab Initio Molecular Orbital Theory*, J. Wiley & Sons, Chichester, **1986**.
[36] P. C. Hariharan, J. A. Pople, *Theor. Chim. Acta* **1973**, *28*, 213–222.
[37] M. M. Francl, W. J. Pietro, W. J. Hehre, J. S. Binkley, M. S. Gordon, D. J. DeFrees, J. A. Pople, *J. Chem. Phys.* **1982**, *77*, 3654–3665.
[38] F. Biegler-König, J. Schönbohm, D. Bayles, AIM2000—A Program to Analyze and Visualise Atoms in Molecules, *J. Comput. Chem.* **2001**, *22*, 545–559.
[39] Xaim: This program was developed by Jose Carlos Ortiz and Carles Bo, Universitat Rovira i Virgili, Tarragona, Spain.
[40] K. Wolinski, J. F. Hinton, P. Pulay, *J. Am. Chem. Soc.* **1990**, *112*, 8251–8260.

Received: September 6, 2007
Published online: February 12, 2008

